THE ASTROPHYSICAL JOURNAL, 481:943–953, 1997 June 1

HARMONIC COUPLING OF THE RED NOISE IN X-RAY PULSARS

L. BURDERI,[1,2] N. R. ROBBA,[1,3] N. LA BARBERA,[1] AND M. GUAINAZZI[3,4]

Received 1996 June 7; accepted 1996 December 9

ABSTRACT

The power spectra of X-ray pulsars often show the presence of a red-noise component. This noise is produced by aperiodic variability believed to be associated with instabilities that seem to occur in accretion flows onto compact objects. In this paper we discuss how, independently of the details of the physical processes that generate these instabilities, a careful analysis of the power spectra can furnish some constraints on the distance from the stellar surface at which the sudden energy release associated with the instabilities occurs. In particular, any aperiodic variability coming from the accretion flow funneled toward the magnetic poles should be modulated at the pulsar spin period (coupling). We show how, in the power spectra, this coupling results in a broadening at the base of the harmonics. To investigate this effect, we have adopted a mathematical description of the noise in order to produce simulated light curves and the resulting power spectra. A comparison of power spectra from simulations with real data allows the detection or exclusion of the broadening effect. As an application of this method we have compared simulated power spectra with one obtained from a *Ginga* observation of the X-ray pulsar SMC X-1. For this source the coupling effect is evident.

Subject headings: methods: statistical — stars: individual (SMC X-1) — stars: magnetic fields — stars: neutron — X-rays: stars

1. INTRODUCTION

Despite the profound differences between the main types of accretion–powered Galactic and extragalactic X-ray sources, a remarkable feature shared by these systems is the presence of aperiodic variability in X-ray light curves. This kind of variability, often referred to as noise because of its random character, has been studied since its detection in the light curve of the black hole candidate Cygnus X-1 observed with the *Uhuru* satellite (Terrell 1972). In particular, the same kind of variability has been reported in several low-mass X-ray binaries (Lewin, van Paradijs, & van der Klis 1988; van der Klis 1989, and references therein) and in a number of X-ray pulsars and black hole candidates (see, e.g., Belloni & Hasinger 1990). The physical processes underlying this kind of phenomenon are still unclear; however, there is general consensus interpreting this variability as a signature of the presence of instabilities in the inflow of matter to the compact source.

On the contrary, only a restricted group of the accreting sources shows periodic behavior that is associated with the rotation of the accretor about its axis. In particular, X-ray pulsators show spin modulation on timescales ranging over 4 orders of magnitude (from 0.069 s of A0538 − 66 to 1455 s of RX J0146 + 619). In these sources the strong magnetic fields of the neutron star funnel the accretion flow toward the magnetic poles. Most of the X-ray luminosity is produced in the magnetically confined accretion columns just above the poles. The rotation of the compact object about its axis produces the so-called lighthouse effect, which modulates the X-ray light curve.

A useful approach in studying both aperiodic and periodic variabilities in X-ray pulsars is the production of power spectral density (PSD) from a fast Fourier transform of the X-ray light curve. In this context the aperiodic variability is indicated by the presence of red noise (RN) in the PSD, a broadband feature in which the power is decreasing toward the high frequencies. Usually the RN shape is a Lorentzian, a power law, a power law with an exponential cutoff, or a combination of power laws with different indices. In addition, more complex features, like bumps and wiggles, are sometimes present over the underlying shape. On the other hand, the periodic variability determines, in the PSD, a family of harmonic lines.

Usually the aperiodic and periodic variabilities are considered separately. For this reason the PSD of an X-ray pulsator is regarded as resulting from the sum of the RN and the harmonic lines. However, this should be regarded as a simplified approach. In fact, if the instabilities that are responsible for the red noise are produced when the accretion flow has already been confined by the magnetic field of the neutron star and brought very close to its surface, the aperiodic variability is modulated by the pulsar spin period. From this point on we refer to this modulation of the aperiodic variability as "coupling." In terms of the Fourier transform this coupling results in the convolution of the RN with the harmonic lines. In the ideal case of an infinite periodic signal the harmonics are represented by a family of δ-functions. In this case the result of the convolution is to place a rescaled version of the RN at the position of each harmonic frequency, mimicking a broadening at the base of the harmonic lines. On the other hand, if the aperiodic variability is generated in regions far away from the stellar surface, where the accreting flow is still unaffected by the magnetic funneling, the periodic and aperiodic features are actually independent and there is no broadening at the base of the harmonic lines. From what is discussed above it is clear that a detailed analysis of the PSD shape at the base of the harmonic lines of an X-ray pulsator could determine whether the aperiodic and periodic features are coupled.

[1] Istituto di Fisica, Università di Palermo, via Archirafi 36-90123, Palermo, Italy.
[2] Astronomy Group, University of Leicester, Leicester LE1 7RH, England, UK.
[3] GIFCO/CNR, Unità di Palermo, via Archirafi 36-90123, Palermo, Italy.
[4] ASI/SAX Science Data Center, via Corcolle 19, I-00131, Rome, Italy.

An analytic derivation of the power spectrum of a signal showing aperiodic variability modulated by a periodic function is described in the Appendix, and the effects of the coupling are shown. However, the finite length of a real light curve introduces a general broadening of each feature in the PSD (due to its convolution with the window function; see Appendix). Moreover, cross terms from the relative phases of the harmonics of the periodic signal arise when the square modulus of the Fourier transform is taken to calculate the power spectra. It is not possible to consider these effects in the analytic derivation, so the formulae obtained are only approximate. With these formulae it is possible to fit the PSD of an X-ray pulsator to search for the coupling effects. Nevertheless, the broadening arising from the coupling effects is mixed with the broadening and interference effects mentioned above, making the results of any fit of the PSD with our approximate analytical expressions not totally conclusive. To overcome this problem we have adopted a more accurate approach. We have simulated finite-length light curves of an X-ray pulsator for different degrees of coupling between the aperiodic component and the periodic modulation. The corresponding PSDs were then produced and compared to that obtained from a real data set. In this way all the effects resulting from a finite length of the signal are properly taken into account.

To this end we have chosen a reliable mathematical description of the aperiodic variability that produces the red-noise component. Although several kinds of processes can, in principle, lead to this kind of feature (such as autoregressive processes or deterministic chaos, as suggested by some authors; e.g., Voges, Atmanspacher, & Scheingraber 1987), the random occurrence of single shots (shot-noise model) is a simple way in which a red noise can be produced. Moreover, fractal analysis of X-ray emission from the X-ray pulsar Centaurus X-3 has been performed to decide the nature of the phenomena that result in the aperiodic variability in X-ray pulsars (Kanetake et al. 1994). The results have shown that the fractal dimension of the X-ray intensity is ≥ 7 when all the variation due to the spin period is removed. This does not fit the idea that the aperiodic variability is caused by global hydrodynamical chaotic oscillations that, typically, are associated with a fractal dimension of 2 or 3, and it seems to indicate that the observed noise is produced by a random superposition of local variability, reinforcing the shot-noise model. In line with this, we have adopted a shot-noise model to describe the aperiodic variability of the X-ray pulsars.

2. INTERACTION OF THE ACCRETING MATTER WITH THE NEUTRON STAR MAGNETIC FIELD

Since the discovery of the first periodically pulsating X-ray binaries Cen X-3 (Giacconi et al. 1971) and Her X-1 (Tananbaum et al. 1972), modulated emission from the X-ray pulsars has been interpreted in terms of accretion on a rotating, magnetized neutron star. The complex physics of accretion onto compact objects, taking into account both the effects of stellar rotation and magnetic fields, has been considered by several authors (e.g., Lamb, Pethick, & Pines 1973). In general, far from its surface the neutron star magnetic field is screened by currents flowing in the highly conducting accreting plasma, while near the star the matter is threatened by the field and forced to corotate with the neutron star. The transition between these two regimes defines the magnetosphere, the zone where the interaction between the accreting matter and the stellar magnetic field takes place. The distance of the magnetosphere from the neutron star is of the order of the Alfvén radius, defined as the point where the energy density of the accreting matter (mainly its kinetic energy) is equal to the energy density of the magnetic field. The plasma penetration through the magnetosphere occurs via instability phenomena. Any energy released (in the form of radiation) during the onset of these instabilities could affect the aperiodic variability. On the other hand, if the accreting flow is already clumpy before the penetration through the magnetosphere, it is important to ask whether these clumps survive to the interaction with the stellar magnetic field until the impact with the neutron star surface.

In the following we briefly review the different mechanisms proposed for the plasma penetration through the magnetosphere and the onset of the instabilities that are typically associated with the interaction of the accretion flow with the magnetic field of the neutron star, suggesting, in some cases, whether the aperiodic variability is expected to be coupled with the neutron star rotation.

The structure of the magnetosphere and the physical processes that drive the plasma penetration through it are strongly dependent on the specific angular momentum of the accreting material respect to the accretor center. If the angular momentum is low enough, the motion of the in-falling plasma is almost radial. The accreting material is stopped by a collisionless shock few hundreds of kilometers above the magnetosphere (Arons & Lea 1976a, 1976b; Elsner & Lamb 1977). The magnetospheric equator is located at a distance equal to the Alfvén radius from the neutron star center. Two cusps are present above the neutron star magnetic poles at a distance half the Alfvén radius. This magnetosphere is stable against plasma penetration unless the plasma undergoes some cooling. In fact, if inverse Compton cooling of the plasma electrons in the radiation bath of the X-rays coming from the stellar surface is effective, Rayleigh-Taylor (interchange) instabilities set in, and the plasma can penetrate the magnetosphere in the form of long diamagnetic filaments and accrete onto the neutron star surface converting its potential energy into X-rays. The growth and the motion of these mushroom-like filaments inside the magnetosphere has been investigated analytically and numerically by several authors (Elsner & Lamb 1977; Ghosh & Lamb 1978; Arons & Lea 1980; Wang & Welter 1982; Wang & Robertson 1984; Wang, Nepveu, & Robertson 1984; Wang & Robertson 1985). The initial motion of these filaments is between the field lines, and, in principle, some of these filaments can fall toward the stellar surface without ever becoming threaded by the field. In this case, the compression of the filaments by the magnetic field can be negligible, and the size of any clumpy feature, close to the neutron star crust crust, could be comparable with the neutron star radius, resulting into accretion onto the whole stellar surface. In this case no spin-modulation effect is expected to arise if the aperiodic variability is associated with the impact of these uncompressed clumps with the neutron star crust. However, Kelvin-Helmholtz (shear) instabilities growing at the filament surfaces can evaporate the filaments, resulting in a threading by the magnetic field lines at the so-called plasmapause surface. In this case, the position of the magnetic field lines tangent to this surface defines, on the neutron star surface, the size of the magnetic caps onto which the matter finally accretes. In this case, if the accretion flow above each magnetic pole is clumpy, the resulting aperiodic variability is strongly modulated at the spin period.

Other penetration mechanisms like accretion via polar cusp diffusion, magnetic field reconnection, or polar cusp descent toward the surface under the effect of gravity have been investigated (Elsner & Lamb 1984). However, in the case of radial inflow and for luminosities $\geq 10^{36}$ ergs s^{-1}, where a significant fraction of the magnetosphere is efficiently illuminated by the X-ray flux, the most efficient penetration mechanism is the onset of Rayleigh-Taylor instabilities. These conditions are typical in the slow-rotating wind-fed high-mass X-ray binaries.

On the other hand, if the specific angular momentum of the accreting material is high enough, the accreting matter orbits the neutron star in a Keplerian accretion disk. In this case, the situation is different (Ghosh & Lamb 1978; Lamb, Pines & Shaham 1978a, 1978b; Ghosh & Lamb 1979; Alpar & Shaham 1985; Lamb et al. 1985; Ghosh & Lamb 1991). As a result of Keplerian centrifugal forces, the effective gravity on the accreting matter is strongly reduced, and consequently interchange instabilities are substantially suppressed. In the extreme case of a perfectly conducting plasma, a diamagnetic disk can be formed outside the magnetosphere. The pressure of this disk deforms the shape of the magnetosphere into an hourglass–like surface, the waist of which is surrounded by the disk. The radius of this waist is about half the Alfvén radius. Different physical processes cause the mixing of the neutron star magnetic field lines and the plasma of the disk, allowing the plasma to penetrate the magnetosphere and accretion to occur. The main processes are Kelvin-Helmholtz instabilities at the interface between the disk and the neutron star field, turbulent diffusion of the magnetospheric field into the disk, and magnetic reconnection of the magnetic loops present in the disk with the neutron star dipole field. The magnetic reconnection scenario has recently been reinvestigated by Aly & Kuijpers (1990). In their model the accretion disk is expected to be broken into small pieces at the accretion radius. In fact, magnetic fields in the disk confine the plasma into blobs carrying magnetic loops which eventually undergo reconnections with the neutron star dipole field. The reconnection phenomena cause a sudden release of magnetic energy in the form of flares, allowing the blob to be loaded onto the stellar field. The subsequent release of angular momentum allows the blobs to spiral in toward the surface. If these flares are associated with the aperiodic variability, no modulation is expected.

3. THE POWER SPECTRAL DENSITY OF AN X-RAY BINARY SIGNAL IN THE SHOT NOISE SCENARIO

Let us consider the characteristics of a signal emitted by a rotating neutron star under the hypothesis that the aperiodic variability is caused by a shot noise process and the periodic variability is due to the stellar spin. The shot noise process arises from the random superposition of shots characterized by a time profile $h(t)$ and a constant mean rate λ. The shot magnitude S is $\int_{-\infty}^{+\infty} h(t)dt$, and the power spectrum of $h(t)$ is $|H(\nu)|^2$.

The most general kind of signal that we consider can be thought as composed of a background component $I_{\rm bck}$ (constant), a uniform component $I_{\rm un}$ (constant), and a shot-noise component $I_{\rm sn}$. Both the uniform component and the shot-noise component can be viewed as the sum of two different contributions: the localized contribution, coming from spots at the neutron star surface (e.g., magnetic poles) and so modulated by the stellar rotation, and the diffuse contribution, coming from well above the surface and so unmodulated. The total intensity of the signal is

$$I_{\rm tot} = I_{\rm bck} + I_{\rm un,DF} + I_{\rm sn,DF} + (I_{\rm un,LC} + I_{\rm sn,LC})M(t) \, .$$

The subscripts "DF" and "LC" indicate the diffuse and the localized components, respectively. The function $M(t)$ is a nonnegative periodic modulation function of arbitrary shape. It represents the lighthouse effect modulation. Therefore, if the occultation of the hot spot is complete, then $M(t) = 0$; moreover, without loss of generality, its maximum value can be always normalized to 1. The period of the modulation function is the neutron star spin period. Its Fourier expansion is $M(t) = C + \sum_k c_k \cos(2\pi k \nu_0 t + \phi_k)$, where ν_0^{-1} is the spin period. The mean intensity of each shot component is related to the shot magnitude and mean arrival rate $I_{\rm sn,DF} = \lambda_{\rm DF} S$ and $I_{\rm sn,LC} = \lambda_{\rm LC} S$. The mean total intensity is

$$\bar{I}_{\rm tot} = I_{\rm bck} + I_{\rm un,DF} + \lambda_{\rm DF} S + C(I_{\rm un,LC} + \lambda_{\rm LC} S) \, . \tag{1}$$

Adopting the Lehay (1983) normalization criterion, the PSD of this signal over a time length T is computed in the Appendix. The calculation gives the following four terms:

$$\begin{cases} \mathrm{P0} = \left(\dfrac{2}{\bar{I}_{\rm tot}}\right) \bar{I}_{\rm tot}^2 [T W_T^2(\nu)] \, , \\ \mathrm{HL} = \dfrac{2}{\bar{I}_{\rm tot}} \displaystyle\sum_k \left(\frac{c_k}{2}\right)^2 [I_{\rm un,LC} + \lambda_{\rm LC} |H(0)|]^2 [T W_T^2(\nu - k\nu_0)] \, , \\ \mathrm{RN} = \left(\dfrac{2}{\bar{I}_{\rm tot}}\right) [\lambda_{\rm DF} |H(\nu)|^2 + \lambda_{\rm LC} C^2 |H(\nu)|^2] \, , \\ \mathrm{CPL} = \left(\dfrac{2}{\bar{I}_{\rm tot}} \displaystyle\sum_k \left(\frac{c_k}{2}\right)^2 \lambda_{\rm LC} |H(\nu - k\nu_0)|^2 \right) \, , \end{cases} \tag{2}$$

where $W_T^2(\nu)$ is the window function (see the Appendix). The meaning of the first term is trivial: the power at zero frequency depends on the integral of the signal, i.e., on its mean intensity. The second term depends on the shape of the modulation function. Any information that can be extracted from this term can be equally extracted by a Fourier expansion of the folded pulse profile. The third term depends on the shot-noise nature of the aperiodic variability. The fourth term depends on the coupling between the shot component and the modulation. This term consists of a series of scaled versions of the RN feature

placed at the position of each harmonic line. The scaling factor is

$$r = \frac{1}{4}\left(\frac{c_k}{C}\right)^2\left(1 + \frac{\lambda_{\rm DF}}{\lambda_{\rm LC}\, C^2}\right)^{-1} . \tag{3}$$

4. THE RED NOISE AS A SHOT NOISE PROCESS

Recent results on PSD analysis of aperiodic variability in 10 X-ray pulsars observed with the *Ginga* satellite (Takeshima, Dotani, & Nagase 1992) have shown that the RN features of these objects exhibit some common features. In the log-log plane it is possible to distinguish two components: a low-frequency component, described by a power law (the slope in the log-log plane is between -1 and -2), and a continuum with a turnover (knee). The slope after the turnover is between -2 and -1 for all sources. These features can be produced by signals composed by a random superposition of shots. This shot-noise model has been used in interpreting the aperiodic X-ray variability of galactic sources and active galactic nuclei (Terrell & Olsen 1970; Terrell 1972; Sutherland, Weisskopf, & Kahn 1978; Priedhorsky et al. 1979). Moreover, shot-noise processes in which the characteristics of each single shot vary according to a statistical distribution has been investigated by some authors (e.g. Halford 1968; Lehto 1989; Burderi et al. 1993; Burderi 1994). In the following we summarize the principal results of this kind of analysis.

A "monochromatic" exponential shot-noise process is obtained from the random superposition of identical, exponentially decaying shots occurring at a constant mean rate λ. Each shot is described by the function $h(t) = U(t)E \exp(-t/\tau)$, where $U(t) = 1$ for $t \geq 0$ and $U(t) = 0$ otherwise. The shot magnitude S is $E\tau$. The power spectrum of the time profile $h(t)$ is

$$|H(\nu)|^2 = \frac{S^2}{1 + (2\pi\tau\nu)^2} .$$

It has a Lorentzian shape (the power spectrum of an exponential) and thus, in a log-log plot, is flat below the knee frequency and has a slope -2 above that frequency. The knee frequency is related to the shot decay time τ via the relation $2\pi\tau\nu_{\rm knee} \sim 1$.

A "colored" exponential shot-noise process is determined when the decay time of the shots is varied according to a statistical distribution, typically a power law, while the shot magnitude S and the mean shot rate λ are kept constant. If this power law is defined over a range of shot decay times $[\tau_{\rm min}, \tau_{\rm max}]$ with power index s, the shape of the resulting power spectrum $|H(\nu)|^2$ depends on the value of s:

1. For $|s| < 1$, the $|H(\nu)|^2$ is characterized by the presence of two knees:

$$\begin{cases} \nu_{\rm min} \sim (2\pi\tau_{\rm max})^{-1} , \\ \nu_{\rm max} \sim (2\pi\tau_{\rm min})^{-1} . \end{cases} \tag{4}$$

$|H(\nu)|^2$, in a log-log plot, is flat well below $\nu_{\rm min}$ and has a slope -2 above $\nu_{\rm max}$. Between the two knees the slope is approximatively

$$\alpha = -(s + 1) . \tag{5}$$

2. For $|s| \gg 1$, the spectrum saturates to the following limit configurations: (i) flat below $\nu_{\rm min}$ and with a slope -2 above it, for $s \gg 1$; (ii) flat until $\nu_{\rm max}$ and with a slope -2 above it, for $s \ll -1$.

In conclusion, the shape of the power spectrum of a colored exponential shot noise for $|s| < 1$ can be approximated by the expression

$$|H(\nu)|^2 \simeq \beta \frac{S^2}{1 + (2\pi\tau_{\rm max}\,\nu)^{\alpha}} ,$$

where

$$\begin{cases} \text{for } \nu \leq \nu_{\rm max}: & \alpha = s + 1 , & \beta = 1 ; \\ \text{for } \nu > \nu_{\rm max}: & \alpha = 2 , & \beta = \dfrac{1 + [\tau_{\rm max}/\tau_{\rm min}]^2}{1 + [\tau_{\rm max}/\tau_{\rm min}]^{(s+1)}} \end{cases} .$$

From the expressions above it is clear that, independently of the "colored" nature of the shot-noise process, the low-frequency limit of $|H(\nu)|^2$ is

$$\lim_{\nu \to 0} (|H(\nu)|^2) = S^2 . \tag{6}$$

The flat shape of $|H(\nu)|^2$ below $\nu_{\rm min}$ puts a further constraint on the detectability of the coupling effects; typically most of the harmonic power is contained in the first few harmonics, and the fact that $r \propto c_k^2$ means that the coupling effects are relevant only for the first harmonic lines. Thus, if significative coupling is present but $\nu_0 \ll \nu_{\rm min}$, the scaled versions of $|H(\nu)|^2$ almost overlap, for the first harmonic lines, with the RN term making the coupling effects undetectable. Actually, in this case, the spin period ν_0^{-1} is longer than the lifetime of the longest shot, $\tau_{\rm max}$, and the shots decay too fast to be efficiently modulated.

5. THE SIMULATION OF THE LIGHT CURVE

In order to simulate the light curves we used Monte Carlo techniques to build up "colored" exponential shot noise. This signal is then added with uniform (constant) components, multiplied by the Fourier expansion of the modulation function $M(t) = C + \sum_k c_k \cos(2\pi k\nu_0 t + \phi_k)$, and then sampled and integrated over the bin size. The result is the vector of the

expected counts per bin. Finally, these numbers are randomized according to Poissonian statistics (that is appropriate for photon detection in a proportional counter). The parameters required to generate the vector of the expected counts per bin can be grouped as

I. ν_0
II. c_k, ϕ_k
III. C
IV. $\tau_{\min}, \tau_{\max}, s$
V. S
VI. $I_{\rm bck}$
VII. $I_{\rm un,DF}, I_{\rm un,LC}$
VIII. $\lambda_{\rm DF}, \lambda_{\rm LC}$

To constrain the parameter space we related some of the quantities above to directly observable quantities.

I: The timing analysis gives very accurate values for ν_0.

II: By folding the light-curve modulo $-\nu_0^{-1}$ an intensity pulse profile $I_{\rm PP}(\psi)$ is obtained, where ψ is the spin phase. The aperiodic variability is averaged to zero by the folding process, and the counting statistics are also improved. The values of c_k and ϕ_k are obtained from a Fourier expansion of the pulse profile.

III: C is constrained between a minimum value, when the minimum of the pulse profile is the actual minimum of the modulation, and a maximum value when no diffuse components are present and the background-subtracted pulse profile is associated with the localized emission.

$$\begin{cases} C_{\min} = \displaystyle\int_0^1 I_{\rm PP}(\psi)d\psi - \min\,\{I_{\rm PP}(\psi) 0 \le \psi \le 1\}\ ; \\ C_{\max} = \displaystyle\int_0^1 I_{\rm PP}(\psi)d\psi\ . \end{cases} \tag{7}$$

Moreover, a relation can be derived from the normalization of $M(t)$: the mean intensity of the modulated component is C times its maximum intensity:

$$\bar{I}_{\rm tot} - (I_{\rm un,DF} + \lambda_{\rm DF} S + I_{\rm bck}) = C[I_{\rm PP\,max} - (I_{\rm DF} + \lambda_{\rm DF} S + I_{\rm bck})]\ , \tag{8}$$

where $I_{\rm PP\,max} = \max\,\{I_{\rm PP}(\psi) 0 \le \psi \le 1\}$.

IV: The shape of the RN feature in the PSD can give information about the decay time of the shots (via the knee frequencies; see eq. [4]) and about their statistical distribution (via the slope of the RN in the log-log representation; see eq. [5]).

V: The low-frequency limit of the RN furnishes a constraint on the magnitude and mean arrival rate of the shots via the relation obtained combining equation (6) with the RN expression in equation (2):

$$\lim_{\nu \to 0} \mathrm{RN} = (2/\bar{I}_{\rm tot})[\lambda_{\rm DF} + \lambda_{\rm LC} C^2] S^2\ . \tag{9}$$

VI: From the data it is always possible to obtain or estimate $I_{\rm bck}$.

VII: An analysis of the third moment of the light curve, similar to that performed for Cygnus X-1 by Sutherland et al. (1978), furnishes the fraction of shot noise present in the entire signal $0 \le F_{\rm sn} \le 1$. This allows to split relation (1) into

$$(1 - F_{\rm sn})(\bar{I}_{\rm tot} - I_{\rm bck}) = I_{\rm un,DF} + C I_{\rm un,LC}\ , \tag{10}$$

$$F_{\rm sn}(\bar{I}_{\rm tot} - I_{\rm bck}) = (\lambda_{\rm DF} + C\lambda_{\rm LC}) S\ . \tag{11}$$

VIII Finally, in line with the physical picture developed in §§ 1 and 2, we considered two cases:

The coupled case, when the aperiodic variability is modulated by the neutron star spin, and the uncoupled case, when the aperiodic variability is not modulated by the spin:

$$\text{coupled:} \begin{cases} \lambda_{\rm DF} = 0\ , \\ \lambda_{\rm LC} \ne 0\ , \end{cases} \qquad \text{uncoupled:} \begin{cases} \lambda_{\rm DF} \ne 0\ , \\ \lambda_{\rm LC} = 0\ , \end{cases}$$

We are left with five unknown quantities in both the coupled and uncoupled case C, S, $I_{\rm un,DF}$, $I_{\rm un,LC}$, and $\lambda_{\rm LC}$ or $\lambda_{\rm DF}$ respectively, and four relations (8), (9), (10), and (11). Furthermore, the parameter C can only range between the limits defined by equation (7). Adopting C as a variable, light curves are simulated for different values spanning the available range. The PSDs of the simulated light curves are computed and compared with the PSD from the data calculating the residuals. As is clear from equation (3), the broadening effect is $\propto C^{-2}$. This strong dependence allows to determine if the coupling is present and, in this case, to calculate C minimising the residuals near the harmonic lines.

6. THE CASE OF SMC X-1

SMC X-1 is a high-mass X-ray binary in the Small Magellanic Cloud. The spin period of the neutron star is 0.717 s. Ground-based observations identified its companion with an early-type B0Ib supergiant (see, e.g., van Paradijs & McClintock 1995). The system shows $\sim$0.6 day X-ray eclipses. The orbit is almost circular ($e \sim 710^{-4}$) with period of 3.892 days and a projected semimajor axis of 53.46 lt-s. Adopting a distance of $\sim$65 kpc, the X-ray luminosity is $\sim 5 \times 10^{38}$ ergs s^{-1}. The

Japanese X-ray satellite *Ginga* observed this source with its proportional counters (Large Area Counters [LAC]) in the energy range 2.3–37.2 keV. We analyzed the observations made in 1989 on July 29 and 31 and on August 1 searching for the signature of the coupling effects. In order to have the maximum number of photons we produced a light curve adding all the energy channels together. The temporal bin size is 62.5×10^{-3} s. The whole data set was divided into intervals containing 8192 points each (corresponding to a time length of $T = 512$ s), and a fast Fourier transform was performed on each of these intervals obtaining 25 PSDs. The PSDs were normalized according to the Lehay at al. (1983) criterion. These PSDs were added together in order to improve the statistics. A white noise (WN) component with power equal to 1.93 was subtracted from the PSD. The WN power is different from the theoretical value of 2, expected from the Lehay normalization, because of dead-time effects. The resulting PSD is shown in Figure 1. An inspection of this figure allows one to identify few components in the PSD:

A low frequency noise (LFN). The LFN is flat between the minimum frequency of the PSD (1.95312510^{-3} Hz) and the turnover frequency of a few 10^{-2} Hz. Then it decreases as a power law (power index ~ -0.75).

A quasi-periodic oscillation component centered at $\sim 10^{-2}$ Hz and with FWHM $\sim 10^{-2}$ Hz (Takeshima 1994).

Five harmonic lines (HL) equally spaced from 1.394700 Hz up to 6.973501 Hz.

A high frequency noise component (HFN) is also evident between $\sim 4 \times 10^{-1}$ Hz and the Nyquist frequency (8 Hz), i.e., roughly in the zone where the harmonic lines are present. This noise component smoothly links to the LFN. Takeshima at el. (1992) have described this noise component as a "continuum with turnover" almost always present in the PSD of X-ray pulsators.

Since in our analysis we are only interested in the study of the aperiodic and periodic components, the whole data set was divided in intervals containing 1024 points each (corresponding to a time of $T = 64$ s). T is chosen in order to have the minimum frequency in the PSD ($1/64$ s^{-1}) just above the QPO frequency. A fast Fourier transform was performed on each of these intervals, obtaining 325 PSDs that were added together and white noise subtracted, resulting in the PSD shown in Figure 2. Our idea is that the coupling effects are so relevant that the whole HFN could result from the coupling effects of the LFN with the periodic modulation. If this is the case, the description of the aperiodic features can be reduced to the presence of the LFN only. In principle, a similar coupling of the QPO feature with the periodic modulation could contribute to the HFN. However, this noise has the shape of a single broad feature extending for few Hz (see Fig. 3). Therefore, the QPO is too

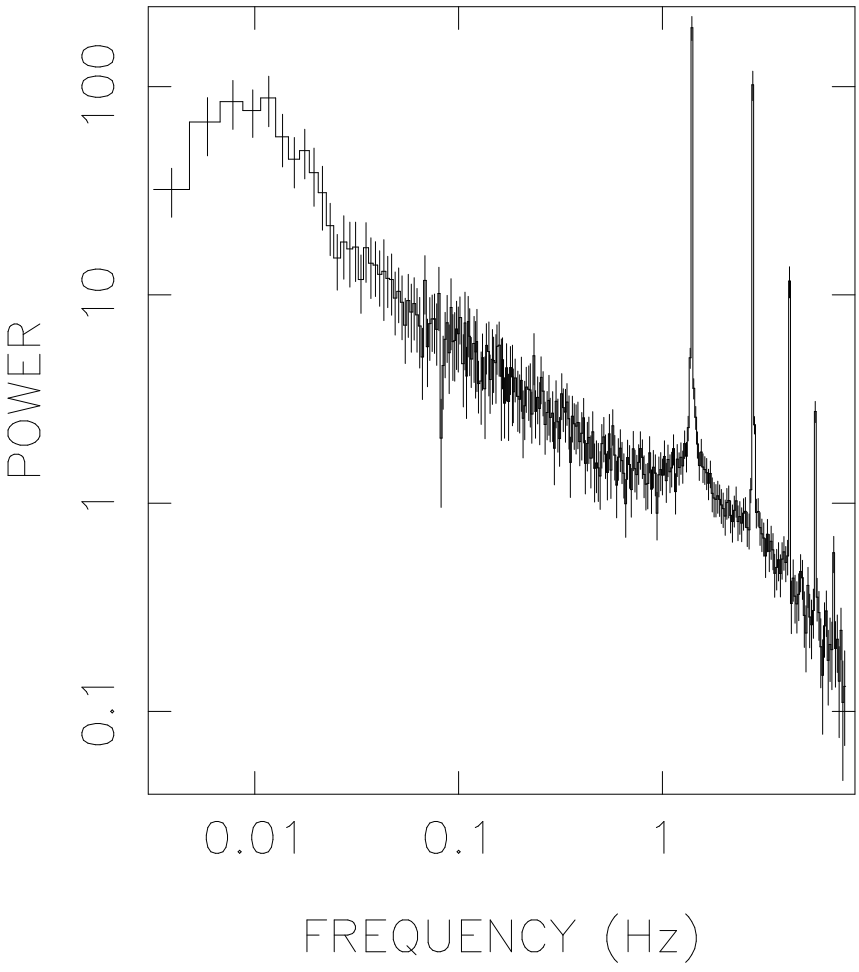

FIG. 1.—PSD of the source SMC X-1 resulting from the sum of 25 PSDs performed on data sets of 512 s each

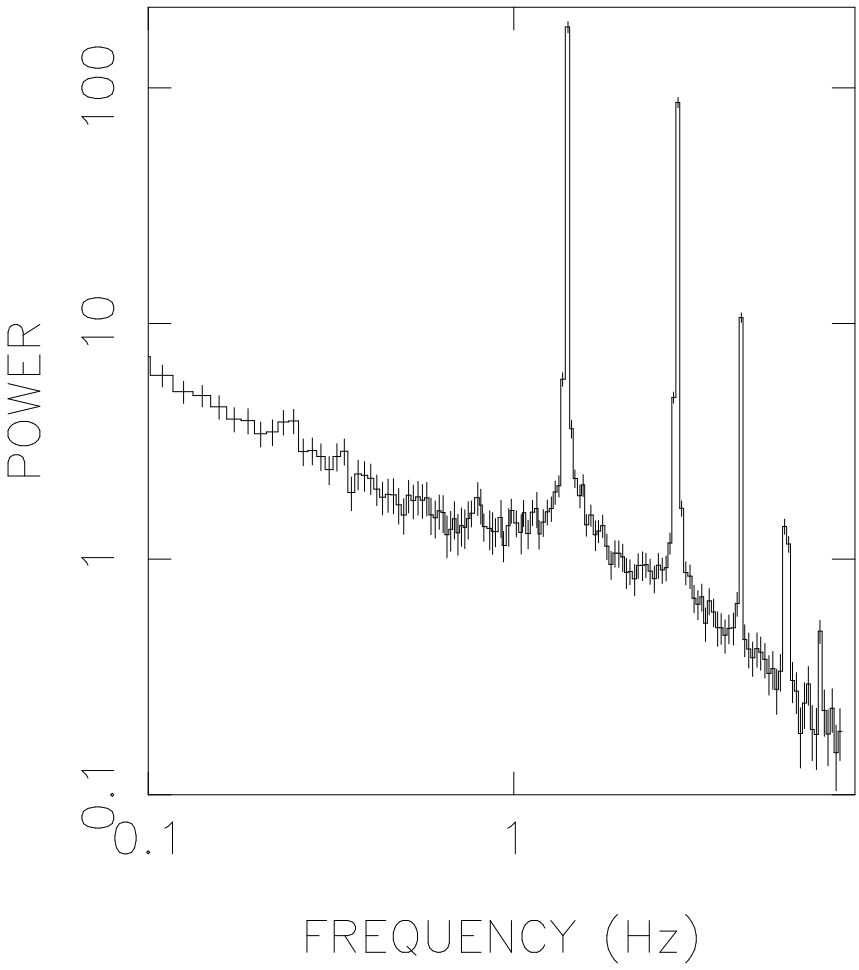

FIG. 2.—PSD of the source SMC X-1 resulting from the sum of 325 PSDs performed on data sets of 64 s each. The points below 0.1 Hz are affected by the presence of the QPO and are not shown.

TABLE 1

PARAMETERS USED FOR SMC X-1 SIMULATIONS

Parameter	Coupled	Uncoupled
Number of PSDs	6100	
Time length of each PSD (s)	64	
Background intensity (photons s^{-1})	40	
Nonshot diffuse intensity (photons s^{-1})	197	138
Diffuse λ (shots s^{-1})	0	1.38
C	0.52	
Nonshot hot-spot intensity (photons s^{-1})	84	211
Hot-spot λ (shots s^{-1})	1.73	0
Shot amplitude (photons)	73	43
Power-law index of the shot distribution law	-0.3	
Minimum τ of the shoots (s)	8×10^{-5}	
Maximum τ of the shots (s)	8	
Number of coherent harmonics	5	
Fundamental frequency (Hz)	1.4085	
Amplitude of the fundamental harmonic	63.17	
Phase of the fundamental harmonic (deg)	19.63	
Amplitude of the first harmonic	64.15	
Phase of first harmonic (deg)	63.93	
Amplitude of the second harmonic	28.12	
Phase of second harmonic (deg)	293.90	
Amplitude of the third harmonic	17.50	
Phase of third harmonic (deg)	253.85	
Amplitude of the fourth harmonic	10.32	
Phase of fourth harmonic (deg)	180.00	

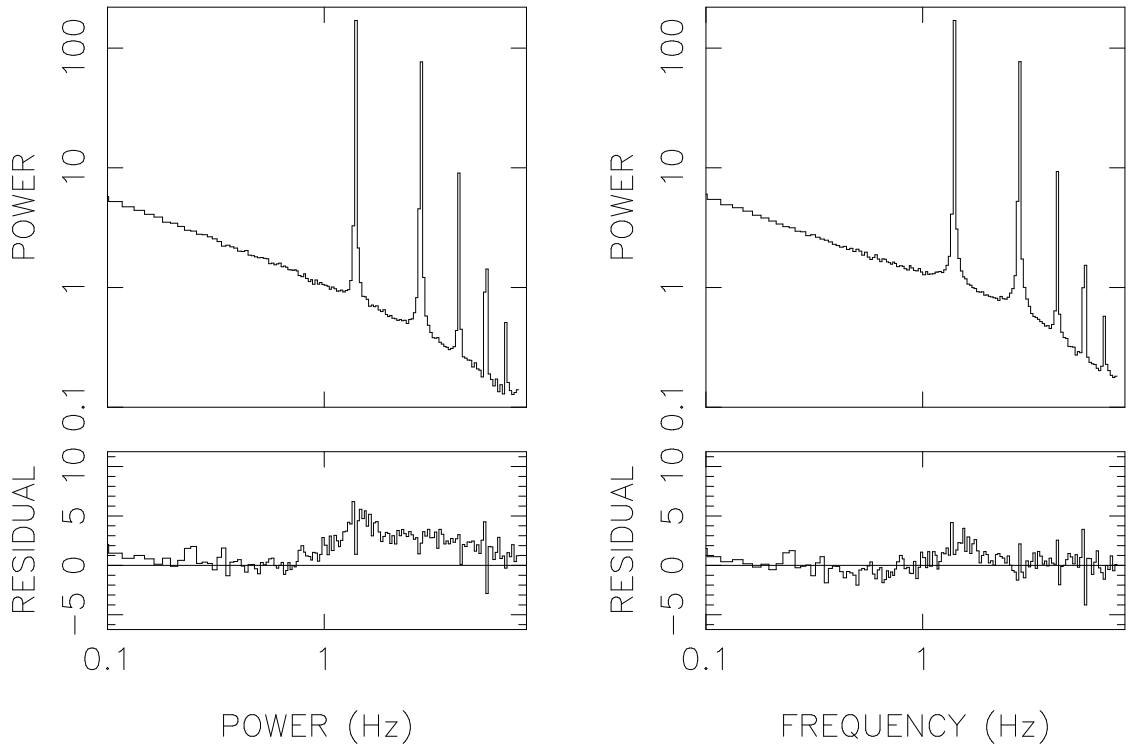

FIG. 3.—*Top panels*: PSDs obtained from the simulated light curves of the source SMC X-1 for the uncoupled (*left*) and coupled (*right*) models. *Bottom panels*: the residual (in units of sigma) resulting from the subtraction of the simulated PSDs from the PSD of Fig.2. The points below 0.1 Hz are are not shown. The small residuals still present at the base of the first harmonic line in the case of coupling could be ascribed to a coupling of the QPO feature with the periodic modulation.

narrow (FWHM $\sim 10^{-2}$ Hz) to give such a smooth broad bump from the blending of the QPO coupling humps corresponding to subsequent harmonics. The LFN feature, in contrast, is broader (FWHM ~ 0.16 Hz) and decreases more slowly (power index ~ -0.75) than the Gaussian QPO. In line with this we neglect, in the following, any possible contribution to the HFN arising from QPO coupling effects. However, a small QPO coupling component seems to be present (see Fig. 3).

We used the simulation method described in the previous section to analyze these data. While the HFN component is evident in the residuals of the uncoupled case (Fig. 3*a*), this feature is absent in the residuals of the coupled case of Figure 3*b*. The parameters used for these simulations are listed in Table 1.

7. DISCUSSION AND CONCLUSIONS

From a comparison of the residuals in both the coupled and the uncoupled case some conclusions can be derived:

The "colored" exponential shot-noise model proposed is quite capable of describing the aperiodic variability associated with the LFN observed in this source. The LFN can be represented by the shot-noise model if we exclude the first few PSD channels around $\nu \sim 1.6 \times 10^{-2}$ Hz, where contamination effects from the QPO present in the real data can significantly distort the shape of the LFN.

The HFN is described by the coupling of the shot noise with the periodic modulation. In principle, the introduction of an extra noise component like the "continuum with turnover" proposed by Takeshima et al. (1992) is also capable of describing the HFN quite well. However, there are two points that make the coupling scenario more attractive. First, the shape of this continuum with turnover is the same of the LFN. This suggests a common origin for both these components, as the coupling scenario predicts. Second, if the LFN is coupled with the HL, one naturally expects that the scaled versions of the LFN are placed at the base of each harmonic line present in the PSD. The consequent blend of these features along the whole system of harmonics mimics a continuum with turnover and naturally places the turnover frequency close to the first harmonic line where is actually observed. In this sense it is possible that one of the results reported by Takeshima et al. (1992) is biased by what is discussed above. In fact, analyzing the PSDs of 10 X-ray pulsars observed by the *Ginga* satellite, they found a very strong one-to-one correlation between the turnover frequency of the HFN and the pulsation frequency in all the pulsars of their sample. In the uncoupled case the origin of this correlation is unclear. On the other hand, the coupling scenario naturally predicts this correlation. A similar conclusion has been recently reached by Lazzati & Stella (1996). The noise model adopted in this paper is a useful mathematical tool to represent the aperiodic variability observed in the X-ray pulsators. However, even considering that a shot-noise process causes the aperiodic variability in these sources, it is quite clear that the "colored" exponential shot noise oversimplifies the physics of the problem. Nevertheless, it is worth stressing that the coupling effects discussed in this paper are quite independent of the nature of the process that originates the aperiodic variability. This is shown in the CPL equation in equation (2) that contains directly the rescaled version of the RN. Moreover, the implication of this coupling is straightforward: independent of the nature of the physical processes that causes the aperiodic variability, the

energy release associated with this phenomenon seems to occur close enough to the surface of the neutron star to be affected by the lighthouse effect that determines the pulsed modulation. In this sense a scenario in which, in line with the Aly & Kuijpers model described in § 2, the shot-noise emission is associated with magnetospheric flares caused by magnetic reconnection all around the magnetosphere cannot work for the origin of the aperiodic variability in this source. In this case, in fact, one expects that the shot component should be totally uncoupled from any periodic modulation. Threading of a inhomogeneous flow by the field (e.g., via Kelvin-Helmholtz instabilities) and subsequent accretion of the blobs onto the polar caps seems a more promising mechanism for the origin of the red noise.

L. B. is supported by the PPARC rolling grant for theoretical astrophysics to the Astronomy Group at the University of Leicester. This research was supported by the Ministero della Ricerca Scientifica e Tecnologica (MURST), and by the Italian Space Agency (ASI).

APPENDIX

THE PSD OF A MODULATED SHOT NOISE SIGNAL

The shot noise is the result of a Poisson process with mean occurrence rate λ,

$$\tilde{z}(\lambda, t) = \sum_i \delta(t - \tilde{t}_i)$$

(here the tilde symbol indicates a random variable; Papoulis 1984) convolved with response functions $h_i(t)$ of arbitrary shape:

$$\mathcal{S}\tilde{\mathcal{N}} = \tilde{z}(t) * h_i(t) = \sum_i h_i(t - \tilde{t}_i) ,$$

where the symbol $*$ denotes convolution (in the following, for simplicity, we will write $\mathcal{SN}$ instead of $\mathcal{S}\tilde{\mathcal{N}}$). Only a few restrictions are imposed on the response functions by the physical nature of the process that generates the shot noise:

There is a general condition of integrability $\int h_i(t)dt = S_i \quad \forall i$.

The functions $h_i(t)$ are nonnegative (the intensity of the signal cannot be less than zero).

Each $h_i(t)$ must satisfy the causality condition $h_i(t) = 0 \quad \forall t < \bar{t}$. This means that each $h_i(t)$ can "exist" starting from a given time $\bar{t}$. Each of these response functions is uncorrelated with each other, and the shot component depends linearly on them. Because of the linearity of the convolution and the lack of correlation between the various response functions, the power spectrum of such a signal is identical, on average, to the power spectrum of a signal obtained from the convolution of $\tilde{z}(\lambda, t)$ with a function $h(t)$ the power spectrum of which $|H(\nu)|^2$ results from averaging the power spectrum of each response function $|H_i(\nu)|^2$ with an appropriate weight function. Thus in this Appendix we consider the shot noise as

$$\mathcal{SN} = \tilde{z}(t) * h(t) = \sum_i h(t - \tilde{t}_i) .$$

The function $h(t)$ is related to the mean intensity of the shot component $\bar{I}_{SN}$ via the relation $\bar{I}_{SN} = \lambda S$, where $S = \int h(t)dt$.

The mean power spectrum of this signal (according to the normalization adopted by Papoulis 1984) can be computed in the framework of the stochastic processes calculus (Papoulis 1984):

$$\mathcal{PS}\{\mathcal{SN}(t)\} = \lambda^2 |H(0)|^2 \delta(\nu) + \lambda |H(\nu)|^2 ,$$

where, by definition, $|H(0)| = \int h(t)dt$ and $\delta(\nu)$ is the Dirac δ-function.

The periodic modulation function $M(t)$ is a train of identical pulse profiles of given period ν_0^{-1}. This means that $M(t)$ can be expanded in a Fourier series:

$$M(t) = C + \sum_k c_k \cos(2\pi\nu_0 kt + \phi_k) .$$

This modulation function represents the lighthouse effect on the emission of the source, so $M(t) \geq 0 \forall t$ and $\max\{M(t'), t' \in [t, t + \nu_0^{-1})\} = 1$. The power spectrum is computed from its definition of square modulus of the Fourier transform $\mathcal{FT}$ over a time interval $T \to \infty$. We made the approximation that the $\mathcal{PS}$ is the sum of the $\mathcal{PS}$ of each Fourier component separately; i.e., we neglect the cross terms that originate performing the square modulus of the Fourier transform. We have (neglecting the negative frequency terms)

$$\mathcal{PS}\{M(t)\} \simeq C^2 \lim_{T\to\infty} \frac{1}{T} |\mathcal{FT}\{\mathcal{BOX}(1, T)\}(\nu - 0)|^2 + \sum_k \left(\frac{c_k}{2}\right)^2 \lim_{T\to\infty} \frac{1}{T} |\mathcal{FT}\{\mathcal{BOX}(1, T)\}(\nu - \nu_k)|^2 ,$$

where $\nu_k = k\nu_0$, the Fourier transforms are computed at the frequencies $\nu = (\nu - 0)$ and $\nu = (\nu - \nu_k)$, respectively, and the box function is defined as

$$\mathcal{BOX}(1, T) = \begin{cases} 1 , & |t| < T/2 , \\ 1/2 , & |t| = T/2 , \\ 0 , & |t| > T/2 , \end{cases}$$

and the square modulus of its Fourier transform is

$$|\mathcal{FT}\{\mathcal{BOX}(1-T)\}(\nu)|^2 = T^2\,\frac{\sin^2(\pi\nu T)}{(\pi\nu T)^2} = T^2 W_T^2(\nu)\ ;$$

$W_T^2(\nu)$ is called the window function. Thus we have

$$\mathcal{PS}\{M(t)\} \simeq C^2 \lim_{T\to\infty} TW_T^2(\nu) + \sum_k \left(\frac{c_k}{2}\right)^2 \lim_{T\to\infty} TW_T^2(\nu-\nu_k)$$

Let us consider a shot noise coupled with a periodic modulation function $\mathcal{SN}(t)\times M(t)$. The Fourier transform of this signal is $\mathcal{FT}\{\mathcal{SN}(t)\times M(t)\} = \mathcal{FT}\{\mathcal{SN}(t)\} * \mathcal{FT}\{M(t)\}$. Performing the convolution with the Fourier transform of the modulation function and neglecting the negative frequency terms, we have

$$\mathcal{FT}\{\mathcal{SN}(t)\times M(t)\} = C\mathcal{FT}\{\mathcal{SN}(t)\}(\nu) + \sum_k \frac{c_k}{2}\,\mathcal{FT}\{\mathcal{SN}(t)\}(\nu=\nu_k)\ .$$

In computing the $\mathcal{PS}$ of the signal we neglect the cross terms, i.e. we compute the $\mathcal{PS}$ of each term separately. So we have

$$\begin{aligned}\mathcal{PS}\{\mathcal{SN}(t)\times M(t)\} \simeq{}& C^2 \lim_{T\to\infty} \frac{1}{T}\,|\mathcal{FT}\{\mathcal{SN}(t)\} * \mathcal{FT}\{\mathcal{BOX}(1,T)\}(\nu)|^2 \\ &+ \sum_k \left(\frac{c_k}{2}\right)^2 \lim_{T\to\infty} \frac{1}{T}\,|\mathcal{FT}\{\mathcal{SN}(t)\} * \mathcal{FT}\{\mathcal{BOX}(1,T)\}(\nu-\nu_k)|^2\ .\end{aligned}$$

Introducing the computed expression for the mean value of the $\mathcal{PS}$ of a shot noise process, we have

$$\mathcal{PS}\{\mathcal{SN}(t)\times M(t)\} \simeq C^2\lambda^2\,|H(0)|^2\,\delta(\nu) + C^2\lambda\,|H(\nu)|^2 + \sum_k \left(\frac{c_k}{2}\right)^2 \lim_{T\to\infty}\frac{1}{T}\,|\mathcal{FT}\{\mathcal{SN}(t)\} * \mathcal{FT}\{\mathcal{BOX}(1,T)\}(\nu-\nu_k)|^2\ .$$

Consider now a signal of the type defined in § 3, i.e.,

$$I_{\rm tot} = I_{\rm bck} + I_{\rm un,DF} + I_{\rm sn,DF} + (I_{\rm un,LC} + I_{\rm sn,LC})M(t)\ .$$

We consider the diffuse (DF) and localized (LC) shot noise components as signals characterized by different arrival rates $\lambda_{\rm DF}$ and $\lambda_{\rm LC}$, and the same response functions $h(t)$ the power spectrum of which is $|H(\nu)|^2$. In calculating the $\mathcal{PS}$ of this signal we neglect, when a pair of terms are uncorrelated, the cross products that average to zero. One of the possible definitions for the distribution $\delta(\nu)$ is $\lim_{T\to\infty} TW_T^2(\nu)$, so adopting this support for the δ functions that appear in the expressions above, we can group all the terms as follows:

$$\begin{cases} \mathcal{PS}_0 = \bar{I}_{\rm tot}^2 \times \lim_{T\to\infty} TW_T^2(\nu)\ , \\ \mathcal{PS}_{\rm lines} = \sum_k \left(\frac{c_k}{2}\right)^2 [I_{\rm un,LC} + \lambda_{\rm LC}\,|H(0)|]^2 \times \lim_{T\to\infty} TW_T^2(\nu-\nu_k)\ , \\ \mathcal{PS}_{\rm rednoise} = \lambda_{\rm DF}\,|H(\nu)|^2 + \lambda_{\rm LC}\,C^2\,|H(\nu)|^2\ , \\ \mathcal{PS}_{\rm coupling} = \sum_k \left(\frac{c_k}{2}\right)^2 \lambda_{\rm LC}\,|H(\nu-\nu_k)|^2\ , \end{cases}$$

where

$$\bar{I}_{\rm tot} = I_{\rm bck} + I_{\rm un,DF} + \lambda_{\rm DF}\,|H(0)| + CI_{\rm un,LC} + C\lambda_{\rm LC}\,|H(0)|$$

is the mean intensity of the signal. The term $\mathcal{PS}_0$, the "zero frequency power," is only dependent on the total intensity of the signal. The term $\mathcal{PS}_{\rm lines}$ is the family of harmonic lines; the term $\mathcal{PS}_{\rm rednoise}$ is the RN feature produced by the shot noise process; finally, the term $\mathcal{PS}_{\rm coupling}$ arises from the coupling of the shot-noise component with the periodic modulation function. This last term is the superposition, at each harmonic, of a rescaled version of the square modulus of the Fourier transform of the response function involved in the shot-noise process. We stress the fact that only the $|H(\nu)|^2$ appears in the last term. This implies that different kinds of signal having the same $|H(\nu)|^2$ would show the same coupling terms.

Let us now compute the value of the squared modulus of the *finite* Fourier transform, i.e., the PSD_T of the signal. We start from the definition of $\mathcal{PS}$

$$\mathcal{PS}\{I_{\rm tot}(t)\} = \lim_{T\to\infty}\left[\frac{1}{T}\,|\mathcal{FT}\{I_{\rm tot}(t)\} * \mathcal{FT}\{\mathcal{BOX}(1,T)\}|^2\right] \simeq \mathcal{PS}_0 + \mathcal{PS}_{\rm lines} + \mathcal{PS}_{\rm rednoise} + \mathcal{PS}_{\rm coupling}\ .$$

To obtain the finite power spectrum $\mathcal{PS}_T$, we have to change from the $\lim_{T\to\infty}$ to a signal of finite length. For the two terms $\mathcal{PS}_{\rm rednoise}$ and $\mathcal{PS}_{\rm coupling}$ some changes occurs in the function $|H(\nu)|^2$. In particular, the new function $|H(\nu)_T|^2$ is a broader version of the old one. The broadening arises from the fact that the window function, which in the infinite power spectrum is a δ-function, is now of the type $TW(\nu)$. Since $H(\nu)$ is already a broadband feature, this convolution gives negligible broadening if

the time length T is not too short. So we can assume

$$|H(\nu)_T|^2 \simeq |H(\nu)|^2 .$$

In the remaining two terms, $\mathcal{PS}_0$ and $\mathcal{PS}_{\rm lines}$, the only modification we have is to eliminate the $\lim_{T\to\infty}$. Thus we define

$$\begin{cases} \mathcal{PS}_{0T} = \bar{I}_{\rm tot}^2[TW_T^2(\nu)] , \\ \mathcal{PS}_{\rm lines\ T} = \sum_k \left(\frac{c_k}{2}\right)^2 [I_{\rm un,LC} + \lambda_{\rm LC}|H(0)|]^2 \times TW_T^2(\nu - \nu_k) , \\ \mathcal{PS}_{\rm rednoise\ T} = \lambda_{\rm DF}|H(\nu)|^2 + \lambda_{\rm LC} C^2 |H(\nu)|^2 , \\ \mathcal{PS}_{\rm coupling\ T} = \sum_k \left(\frac{c_k}{2}\right)^2 \lambda_{\rm LC}|H(\nu - \nu_k)|^2 . \end{cases}$$

With these definitions we have

$$|a_T(\nu)|^2 = T\mathcal{PS}_T\{I(t)\} = |\mathcal{FT}\{I(t)\} * \mathcal{FT}\{\mathcal{BOX}(1, T)\}|^2 \simeq T[\mathcal{PS}_{0T} + \mathcal{PS}_{\rm lines\ T} + \mathcal{PS}_{\rm rednoise\ T} + \mathcal{PS}_{\rm coupling\ T}] .$$

Finally, adopting the Lehay's normalization factor $2/[a_T(\nu = 0)]$, with $a_T(\nu = 0) = \bar{I}_{\rm tot}\, T$, we have

$$PSD_T(\nu) = \frac{2}{a_T(\nu = 0)}|a_T(\nu)|^2 \simeq \frac{2}{\bar{I}_{\rm tot}}[\mathcal{PS}_{0T} + \mathcal{PS}_{\rm lines\ T} + \mathcal{PS}_{\rm rednoise\ T} + \mathcal{PS}_{\rm coupling\ T}] = P0 + HL + RN + CPL .$$

We observe that the strength of the two terms $\mathcal{PS}_{0T}$ and $\mathcal{PS}_{\rm lines\ T}$ that relate to coherent processes grows linearly with T, while the strength of the aperiodic processes $\mathcal{PS}_{\rm rednoise,T}$ and $\mathcal{PS}_{\rm coupling,T}$ that relate to intrinsically incoherent processes does not grow with the signal duration.

REFERENCES

Alpar, M. A., & Shaham, J. 1985, Nature, 316, 239
Aly, J. J., & Kuijpers, J. 1990, A&A, 227, 473
Arons, J., & Lea, S. M. 1976a, ApJ, 207, 914
———. 1976b, ApJ, 210, 792
———. 1980, ApJ, 235, 1016
Belloni, T., & Hasinger, G. 1990, A&A, 230, 103
Burderi, L. 1994, Ph.D. thesis
Burderi, L., Robba, N. R., Guainazzi, M., & Cusumano, G. 1993, Il Nuovo Cimento, 16C, 5
Elsner, R. F., & Lamb, F. K. 1977, ApJ, 215, 987
———. 1984, ApJ, 278, 326
Ghosh P., & Lamb, F. K. 1978, ApJ, 223, L83
———. 1979, ApJ, 232, 259
———. 1991, in Neutron Stars: Theory and Observation, ed. J. Ventura & D. Pines (Dordrecht: Kluwer), 363
Giacconi, R., et al. 1971, ApJ, 167, L67
Halford, D. 1968, Proc. IEEE, 56, 251
Kanetake, R., et al. 1994, PASJ, 46, 235
Lamb, F. K., Pethick, C. J., & Pines, D. 1973, ApJ, 184, 271
Lamb, F. K., Pines, D., & Shaham, J. 1978a, ApJ, 224, 969
———.1978b, ApJ, 225, 582
Lamb, F. K., et al. 1985, Nature, 317, 681
Lazzati, D., & Stella, L. 1996, ApJ, in press
Leahy, D. A., et al. 1983, ApJ, 266, 160
Lehto, H. J. 1989, Proc. 23rd ESLAB Symposium, ed. N. E. White (Noordwijk: ESA), 499
Lewin, A., van Paradijs, J., & van der Klis, M. 1988, Space Sci. Rev., 46, 273
Papoulis, A. P. 1984, Probability, Random Variables and Stochastic Processes (2nd ed.; Singapore: McGraw-Hill)
Priedhorsky, W., et al. 1979, ApJ, 233, 350
Sutherland, P. G., Weisskopf, M. C., & Kahn, S. M. 1978, ApJ, 219, 1029
Takeshima, T. 1994, Ph.D. thesis
Takeshima, T., Dotani, T., & Nagase, F. 1992, in Frontiers of X-Ray Astronomy (Universal Acad. Press)
Tananbaum, H., et al. 1972, ApJ, 174, L143
Terrell, J., & Olsen K. H. 1970, ApJ, 161, 399
Terrell, N. J., Jr. 1972, ApJ, 174, L35
van der Klis, M. 1989, AAR&A, 27, 517
van Paradijs, J., & McClintock, J. E. 1995, in X-Ray Binaries, ed. W. H. G. Lewin, J. van Paradijs, & E. P. J. van den Heuvel (Cambridge: Cambridge University Press)
Voges, W., Atmanspacher, H., & Scheingraber, H. 1987, ApJ, 320, 794
Wang, Y. M., Nepveu, M., & Robertson, J. 1984, A&A, 135, 66
Wang, Y. M., & Robertson J. A. 1984, A&A, 139, 93
———. 1985, ApJ, 299, 85
Wang, Y. M., & Welter, G. M. 1982, ApJ, A&A, 113, 113